ADVANCED OPTICAL MATERIALS
www.advopticalmat.de

Flexible Confinement and Manipulation of Mie Resonances via Nano Rectangular Hollow Metasurfaces

Zhancheng Li, Guangzhou Geng, Jiaqi Cheng, Wenwei Liu, Shiwang Yu, Boyang Xie, Hua Cheng,* Junjie Li,* Wenyuan Zhou, Jianguo Tian, and Shuqi Chen**

Mie resonances excited in high-index all-dielectric metasurfaces provide a powerful platform for the constraint and manipulation of light at the subwavelength scale, which enable tremendous advanced developments in optical field manipulation, imaging, and sensing. Recently, how to manipulate and confine Mie resonances in the frequency domain has attracted tremendous interest since it is invaluable for the implementation of frequency-selective and -multiplexed optical devices. Here, the authors theoretically analyze and experimentally demonstrate that the nano rectangular hollow (NRH) metasurfaces are promising candidates for the flexible confinement and effective manipulation of Mie resonances in the frequency domain. They reveal that the diameter of the hollow in the NRH can provide an efficient degree of freedom for the constraint of displace currents in the space domain, which results in the confinement of Mie resonances in the frequency domain. The excitation wavelength of the Mie resonance can also be manipulated by adjusting the side length of the NRH. The potential uses of NRH metasurfaces in the implementation of frequency-selective intensity encoding and optical encryption are theoretically and experimentally demonstrated. The results provide a fertile ground for confining Mie resonances in the frequency domain and can be further applied in frequency-multiplexed optical devices.

1. Introduction

Low-loss dielectric metasurfaces with both electric and magnetic Mie resonances emerged as a feasible platform for high-efficient optical wave manipulation in the recent years.[1–3] The excitation of Mie resonances in dielectric nanostructures is due to the coupling between the incident optical waves and the displacement currents within the nanostructures induced by the field penetration and phase retardation inside the nanostructures.[4] The Mie resonance can appear if the characteristic size of the dielectric nanostructure is about λ/n (n is the refractive index of the dielectric material). Therefore, the materials with high refractive indexes are essential for the excitation of Mie resonances in the visible and near-infrared regimes.[5] As the resonant wavelength, the field penetration, and phase retardation within the dielectric nanostructures are related with the structural parameters, the Mie resonance of dielectric metasurfaces can be directly manipulated by changing the structural parameters. As a result, dielectric metasurfaces show unprecedented capacities for both near- and far-field optical wave manipulation with a high degree of freedom.[4–9] They have promoted a rapid development of metaphotonics and have been widely used for wavefront manipulation,[10,11] metahologram,[12,13] nonlinear harmonic generation,[14–16] structural color,[17,18] imaging,[19,20] and sensing.[21]

Recently, realizing the confinement of Mie resonances in the frequency domain has attracted more and more attention from researchers, since dielectric nanostructures with controllable resonance bandwidth are highly desirable for the production of saturated structural colors,[22] the ultrasensitive optical sensing,[23] and the implementation of frequency-multiplexed optical devices.[13,24,25] One and the most popular way of confining Mie resonances in the frequency domain is utilizing the advanced effects, such as the quasi-bound states in the continuum and the anapoles, caused by coupling and interference of different resonant modes in one or multiple dielectric nanostructures.[26–28] Although, optical resonances with high quality factors and significantly enhanced local fields have been well realized with this method. There are still some major limitations of this method. The designed optical resonances can be easily influenced by the loss of dielectric materials and

Z. Li, G. Geng, J. Cheng, W. Liu, S. Yu, B. Xie, H. Cheng, W. Zhou, J. Tian, S. Chen
The Key Laboratory of Weak Light Nonlinear Photonics
Ministry of Education
Renewable Energy Conversion and Storage Center
School of Physics and TEDA Institute of Applied Physics
Nankai University
Tianjin 300071, China
E-mail: byxie@nankai.edu.cn; hcheng@nankai.edu.cn; schen@nankai.edu.cn

J. Li
Beijing National Laboratory for Condensed Matter Physics
Institute of Physics
Chinese Academy of Sciences
Beijing 100190, China
E-mail: jjli@iphy.ac.cn

S. Chen
The Collaborative Innovation Center of Extreme Optics
Shanxi University
Taiyuan, Shanxi 030006, China

S. Chen
Collaborative Innovation Center of Light Manipulations and Applications
Shandong Normal University
Jinan, Shandong 250358, China

The ORCID identification number(s) for the author(s) of this article can be found under https://doi.org/10.1002/adom.202200185.

DOI: 10.1002/adom.202200185

the variation of the structural parameters, resulting in a low performance of the fabricated samples. The high-quality factor of the optical resonances will result in an ultranarrow resonant bandwidth, preventing their application in color-multiplexed optical devices. The other way is utilizing dielectric metasurfaces composed of stacked-layer nanostructures with antireflection effect, in which the refractive index distribution along the wave propagation direction is modulated by changing the thickness of the stacked-layer composed of different dielectric materials, resulting in the suppression of the Mie resonances in the short wavelengths.[29] The optical resonances obtained with this method have a wider resonant bandwidth, which were used for the production of ultrahighly saturated structural colors. The main drawback of this approach is that the thickness of the stacked-layer need to be specifically designed, resulting in a high requirement on fabrication technology. Therefore, an effective approach for the realization of confining and manipulating Mie resonances in the frequency domain, need to be newly presented.

Here, we demonstrate that the nano rectangular hollow (NRH) metasurfaces can be used to flexibly confine and effectively manipulate the Mie resonances in the frequency domain. We reveal that the nano hollows in the NRH metasurfaces can well constraint the displacement currents in the space domain, resulting in the suppression of the Mie resonances in the short wavelength and the rapid decrease of the resonant strength with the change of wavelength. We theoretically and experimentally prove that the resonant wavelength and bandwidth of the NRH metasurfaces can be exactly manipulated by changing the side length and the hollow diameter of the NRH respectively. The great potential of NRH metasurfaces for frequency-selective intensity manipulation and optical encryption has also been experimentally validated. Our results provide a good alternative for the realization of Mie resonances with narrow bandwidth.

2. Results and Discussion

Figure 1 illustrates the flexible confinement of Mie resonances in the frequency domain via changing the diameter S of the hollow in the TiO_2 nano rectangular cuboids on a SiO_2 substrate. The resonance bandwidth decreases with the increase of the diameter of the nano hollow. Since the refractive index of TiO_2 is sufficiently high and its loss can be negligible compared with Si and GaAs in the visible regime, we choose TiO_2 as the constituent material of the NRHs to support Mie resonances. The proposed NRH metasurfaces can be fabricated by using our recently developed nanofabrication method—the atomic layer assembling fabrication (ALAF) method.[30] The top surface of the fabricated nanostructure based on ALAF method is uneven. Therefore, the structural configurations of NRH metasurfaces for theoretical analysis were obtained by considering the fabrication tolerance. The side length of NRH l, the diameter of the hollow S, the height of the rectangular hollow t, the period of a unit cell P, and the height of the NRH t_0 without the edge are the structural parameters of the designed NRH metasurfaces. We define the width of the side wall as $w = (l - S)/2$, then the angle θ can be expressed as $\arctan((t - t_0)/w)$.

To reveal the advantages of NRH metasurfaces on Mie resonance confinement in the frequency domain, we implemented a quantitative analysis by making a comparison between the NRH metasurfaces and the nanoblock metasurfaces. **Figures 2**a and 2b show the simulated transmission and reflection spectra of a nanoblock metasurface and a NRH metasurface under the x-polarized normal illumination, respectively. The structural parameters of the nanoblock and the NRH metasurfaces are: $l = 160$ nm, $P = 250$ nm, $t = 250$ nm and $t_0 = 210$ nm, $S = 0$ nm for the nanoblock metasurface and $S = 80$ nm for the NRH metasurface. The resonance of the NRH metasurface can be confined in a narrower bandwidth (half-peak width is 9.8 nm

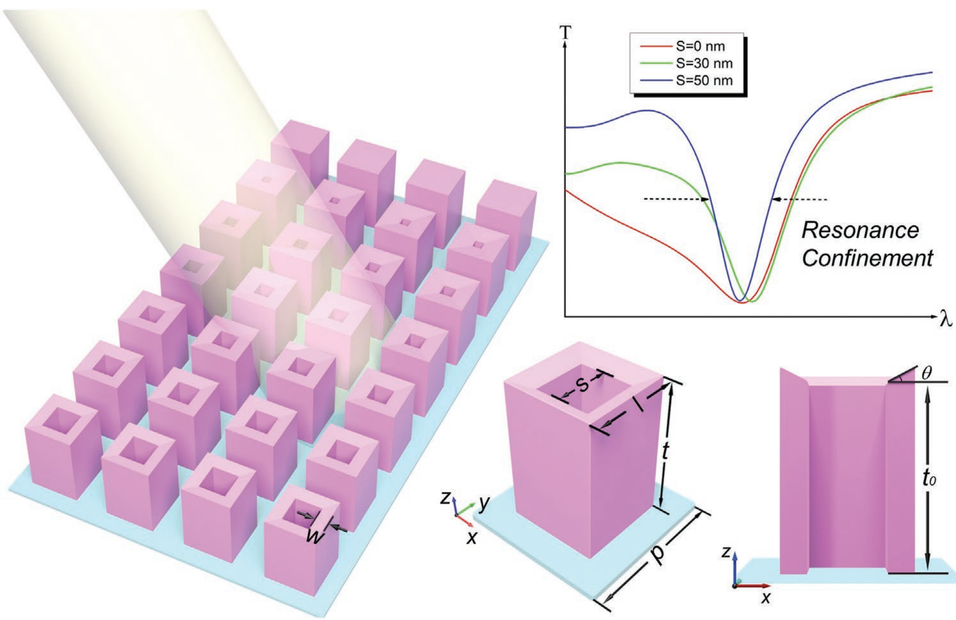

Figure 1. Schematic illustrating the Mie resonance confinement in the frequency domain via the proposed NRH metasurfaces and the structure configuration of the proposed NRH metasurfaces.

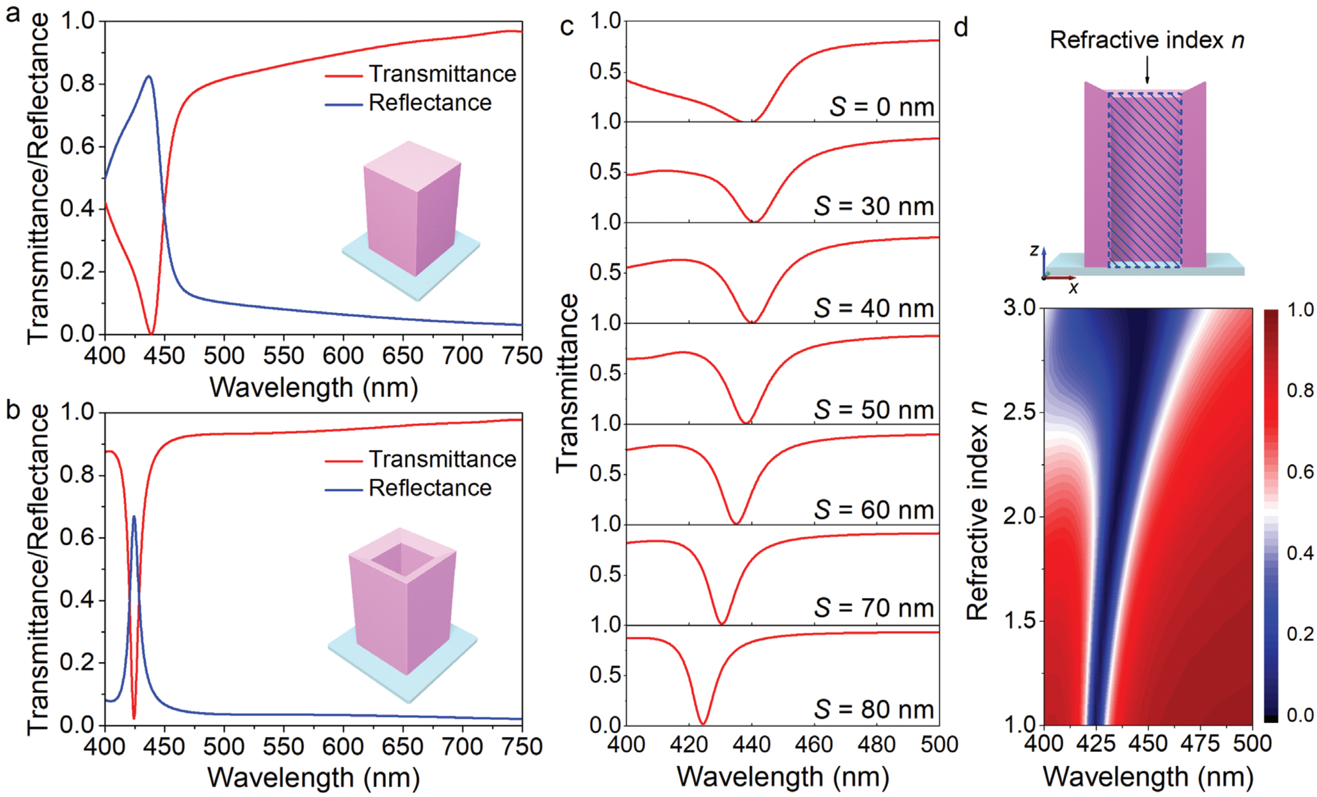

Figure 2. The implementation of Mie resonance confinement in the frequency domain via NRH metasurfaces. Simulated transmission and reflection spectra of TiO_2 dielectric metasurfaces composed of a) nanoblocks and b) NRHs. c) The variation of transmission spectra of the NRH metasurface with the changing of the hollow diameter S, while the structural parameter l = 160 nm. The NRH metasurface with S = 0 nm can be regarded as a metasurface composed of nanoblocks. d) Schematic of the NRH metasurface (l = 160 nm, S = 80 nm, t = 250 nm, t_0 = 210 nm, and p = 250 nm) in which the refractive index n in the hollow (blue shaded area) is changed from 1.0 to 3.0 in the simulation, and the corresponding simulated transmission spectra as a function of the refractive index n.

with a center wavelength of 424.3 nm) when compared with that of the nanoblock metasurface with the same structural parameters. We further investigated the resonant bandwidths of the NRH metasurfaces with different diameters S of the nano hollow in Figure 2c. The resonances in short wavelengths are gradually suppressed with the increasing of S, resulting in the decrease of the resonant bandwidth. We calculated the quality factors for NRH metasurfaces with different S based on the simulated transmission spectra: $Q = \omega_r/\Delta\omega$, where ω_r is the angular resonant frequency and $\Delta\omega$ is the full width at half maximum. The quality factors for NHR metasurfaces with S = 0, 30, 40, 50, 60, 70, and 80 nm are 6.8, 15.0, 20.2, 25.1, 30.0, 36.4, and 43.3, respectively. Therefore, the diameter S of the nano hollow provides an effective degree of freedom for the flexible confinement of Mie resonances in the frequency domain. The current density within the dielectric nanostructures, which correlated to the excitation of Mie resonance, can be expressed as:[31]

$$\mathbf{J}(\mathbf{r}) = i\omega\varepsilon_0(\tilde{\varepsilon}_r - 1)\mathbf{E}(\mathbf{r}) \tag{1}$$

where ω, ε_0, $\tilde{\varepsilon}_r$ and $\mathbf{E}(\mathbf{r})$ are the angular frequency of light field, the free-space permittivity, the complex-valued dielectric constant, and the electric field in space position $\mathbf{r}$. The variation of the diameter S of the nano hollow can lead to the change of the permittivity distribution within the plane and the constraint of the displacement currents, which results in the confinement of Mie resonances in the frequency domain. To make a further validation, we investigate the influence of the refractive index of the nano hollow area on the resonance of the NRH metasurfaces in Figure 2d. The resonance is confined in a narrow bandwidth when the refractive index of the nano hollow area equals to 1. With the increase of the refractive index of the nano hollow area, the current density in the nano hollow area is no longer equal to zero and the bandwidth of the resonance significantly widens. The variation trends of the transmission spectra with the changing of the structural parameter S and the refractive index of the nano hollow area are consistent with each other. Therefore, the confinement of Mie resonances in the frequency domain in the proposed NRH metasurfaces is directly related to the constraint of the displacement current in the space domain, and both the refractive index and the diameter of the nano hollow area play a dominate role for the confinement of Mie resonances.

To make a deep insight on the physical mechanism for the implementation of Mie resonance confinement in the NRH metasurfaces, we utilize the electromagnetic multipole expansion method to further analyze the resonance modes for both of the nanoblock and NRH metasurfaces, whose transmission and reflection spectra are shown in Figure 2a,b. Based on the

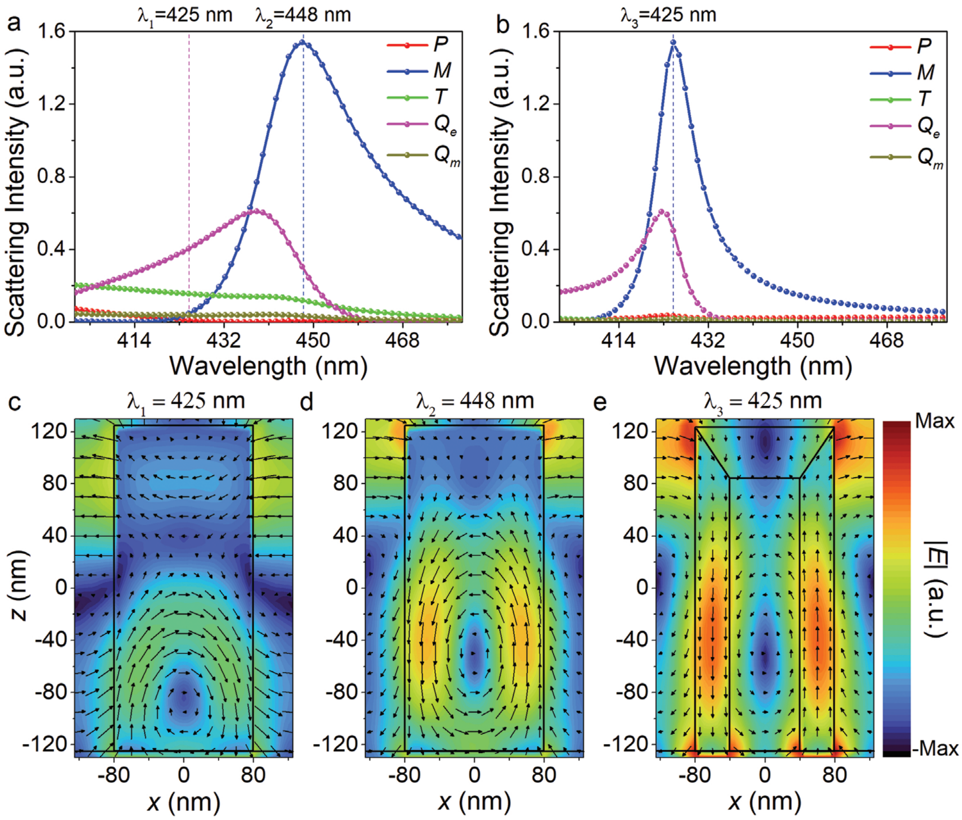

Figure 3. The resonant modes in nanoblock and NRH metasurfaces. Multipolar decomposition of the scattering power spectra of TiO_2 dielectric metasurfaces composed of a) nanoblocks and b) NRHs in terms of electric dipole (*P*), magnetic dipole (*M*), toroidal dipole (*T*), electric quadrupole (Q_e), and magnetic quadrupole (Q_m) under the *x*-polarized illumination. Simulated results of the electric field flows (black arrows) and the electric field amplitude distribution in the *x*–*z* plane ($y = 0$ nm) at c) $\lambda_1 = 425$ nm, d) $\lambda_2 = 448$ nm for the nanoblock metasurface, and at e) $\lambda_3 = 425$ nm for the NRH metasurface.

electromagnetic multipole expansion method, the scattering intensity of each electromagnetic multipole can be expressed as:[32,33]

$$= \frac{2\omega^4}{3c^3}|\mathbf{P}|^2 + \frac{2\omega^4}{3c^3}|\mathbf{M}|^2 + \frac{2\omega^6}{3c^5}|\mathbf{T}|^2 + \frac{\omega^6}{5c^5}\Sigma\left|Q_{\alpha\beta}^{(e)}\right|^2 + \frac{\omega^6}{40c^5}\Sigma\left|Q_{\alpha\beta}^{(m)}\right|^2 + \ldots \tag{2}$$

where α, $\beta = x, y, z$. The terms represent the components of electric dipole (**P**), magnetic dipole (**M**), toroidal dipole (**T**), electric quadrupole ($\mathbf{Q}^{(e)}$), and magnetic quadrupole ($\mathbf{Q}^{(m)}$), respectively. The multipolar decompositions of the scattering power spectra for the nanoblock and NRH metasurfaces are shown in **Figures 3**a and 3b, respectively. The results indicate that the valleys in the transmission spectra in Figure 2a,b are mainly attributed to the excitations of the magnetic dipole and the electric quadrupole. Therefore, the Mie resonances in the NRH metasurface can remain almost unchanged under the TE illumination, while it is very sensitive to the changes in the incident angle under the TM illumination (details in Figure S1, Supporting Information). Compared with the nanoblock metasurface, the strength of resonance in the NRH metasurfaces decreases faster with the change of wavelength because the displacement current is constrained in the TiO_2 nanostructure. To further prove this conclusion, we simulated the electric field flows and amplitude distribution in the *x*–*z* plane ($y = 0$ nm) at three different wavelengths for the two metasurfaces under the *x*-polarized normal illumination, as shown in Figure 3c–e. For the nanoblock metasurface, the resonance at 425 nm is mainly composed of an electric quadrupole in the *x*–*z* plane and a toroidal dipole along the *x*-axis, while the resonance at 448 nm is mainly related to a magnetic dipole. For the NRH metasurface, the resonance at 425 nm is mainly attributed to the magnetic dipole. These results are in good agreement with the quantitative analysis in Figure 3a,b. As shown in Figure 3e, the displacement currents in the NRH metasurface are enhanced and constrained in the TiO_2 thin-wall, resulting in a pair of antiparallel currents along the *z*-axis that correspond to the excitation of a magnetic dipole in the *y* direction (details in Figure S2, Supporting Information). Hence, the narrower resonant bandwidth of NRH metasurface can be mainly attributed to the following reasons. The displacement currents are constrained within the thin side walls for the NHR metasurfaces with small side wall thickness *w*. For a given resonant mode, the regional distribution of displacement currents inside the nanostructures is wavelength dependent. Therefore, the strength of resonances at off center resonant wavelengths in NRH metasurfaces is significantly suppressed when compared with those in nanoblock metasurfaces. Meanwhile, the resonances of the nanoblock metasurface at the short wavelengths are mainly attributed to the electric quadrupole with an

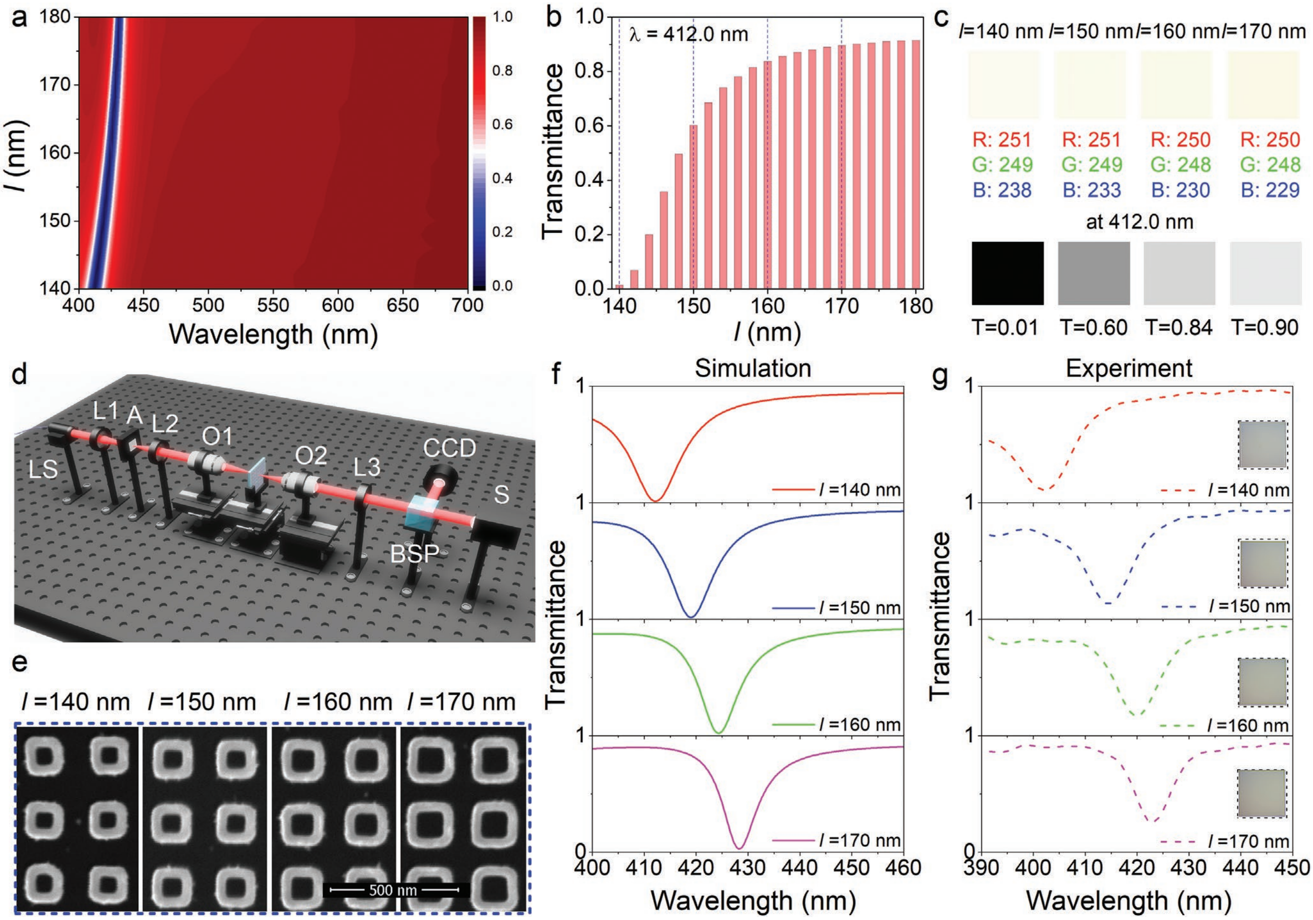

Figure 4. Manipulating the resonant wavelengths of NRH metasurfaces via changing structural parameter l. a) Simulated results of the transmission spectra variation of the NRH metasurface with the changing of length l, while w = 40 nm. b) Simulated results of transmission intensity as a function of l at 412 nm for NRH metasurfaces. c) Simulated results of the color images (and the corresponding RGB values), and the gray images (and the corresponding transmission intensities) at 412 nm of periodic NRH metasurfaces with different lengths l. The color images were calculated with D50 light source and the viewing angle is 10°. The wavelengths 412 nm is the valley values of the transmission spectrum of the proposed NRH metasurface with l = 140 nm. d) Schematic of the home-built experimental setup: LS: light source (bromine tungsten lamp); L: lens; A: aperture slot; O: Objective; BSP: unpolarized beam splitting prism; CCD: charge coupled device camera; S: spectrograph. e) SEM images of the fabricated periodic NRH metasurfaces with different lengths l. f) Simulated and g) measured results of the transmission spectra of NRH metasurfaces with different lengths l. Inset: Captured color images of the periodic NRH metasurfaces.

enhanced electric field in the center of the nanoblock (as shown in Figure 3c and Figure S3, Supporting Information). Changing the material of the center of the nanoblock from TiO_2 to air will significantly suppress the resonance in the short wavelength. A comprehensive comparison between the proposed NRH metasurface and the previous designs for the implementation of Mie resonances with narrow resonant bandwidth can be found in Table S1, Supporting Information. It should be pointed out that the NRH metasurface cannot confine the electric dipole resonance in the frequency domain, for which the Mie-resonance-induced displacement currents are mainly excited in the center of the nanoblocks. As a result, the proposed NRH metasurfaces also provide a good approach for the mode-selective excitation of Mie resonance.

In addition to the diameter S of the hollow (the width w of the side wall), the side length l can be used to manipulate the Mie resonance in the frequency domain, which has been widely applied in the production of structural colors.[17,29] We further analyze the influence of the structural parameter l on the resonance of the NRH metasurface by fixing the width w of the side wall. **Figure 4**a shows the simulated transmission spectra of the NRH metasurfaces with different l and the same w = 40 nm, respectively. The resonant wavelength has a red shift with the increase of l, while the shift of the peak for the NRH metasurface is smaller than that for the nanoblock metasurface (details in Figure S4, Supporting Information). We also investigate the variation of the transmission intensity with the changing of l at 412 nm (corresponding to the valley value of the transmission spectra when l = 140 nm), as shown in Figure 4b. The transmission intensity of the NRH metasurface at 412 nm undergoes significant change from 0.01 to 0.60 when the length l changes from 140 to 150 nm. The results in Figure 4a,b prove that the NRH metasurface is a good alternative for the implementation of frequency-selective intensity encoding and optical encryption.[33,34] Specifically, as shown in Figure 4c, the color of the NRH metasurface remains almost unchanged with the variation of l, while the transmission intensity changes from 0 to 0.90 at 412 nm. On the contrary, the color of the nanoblock metasurface significant changes with the variation of l (details in Figure S4c, Supporting Information). Therefore, the NRH metasurface with different l and a given w can be utilized to realize the multilevel intensity encoding at a particular wavelength, while the encoded information can be hardly recognized under the white illumination. Moreover, the resonant wavelength of the NRH metasurface can be continuously modulated in the whole visible regime by changing both l and P at the same time as the structural parameter P can also manipulate the resonant wavelength (Figures S5 and S6, Supporting Information), which promises the potential application of NRH metasurfaces for the generation of structural colors. To make an experimental validation of the above discussed outstanding features of the NRH metasurface, we first measured the transmission spectra of the NRH metasurfaces with different l and a given w = 40 nm. The transmission spectra were measured by using a home-built experimental setup, as shown in Figure 4d. The details of the experimental setup and the sample fabrication process can be founded in the Experimental Section. Figure 4e shows the SEM images of the fabricated samples with different lengths l. The simulated and measured transmission spectra and color images of the NRH metasurfaces with different l are shown in Figure 4f,g, which are in good agreement with each other. The measured color images validate that the color of the NRH metasurface can remain almost unchanged with the variation of l. The measured transmission spectra show slight blue shifts compared with the simulated ones, which can be attributed to the fabrication errors of the structure edges. Note that the resonant wavelength of the NRH metasurface can also be modulated by changing the width w of the side wall while fixing the diameter S of the nano hollow. For a NRH metasurface with a fixed S and a large w, the situation is the same as a NRH metasurface with a fixed l and a small S. Therefore, when S is fixed, the resonant linewidth will increase with the increase of w, and the unwanted resonances in the short wavelengths cannot be well eliminated, resulting in a poor performance on resonance confinement in the frequency domain. Aperiodic metasurfaces composed of NRHs with different width w of sidewall cannot be easily fabricated by utilizing the ALAF method. Hence, the proposed strategy on Mie resonance manipulation in the frequency domain is also built with the consideration of the manufacturability of the designed NRH metasurfaces.

We further make an experimental validation of the capacities of the NRH metasurface for the frequency-selective optical

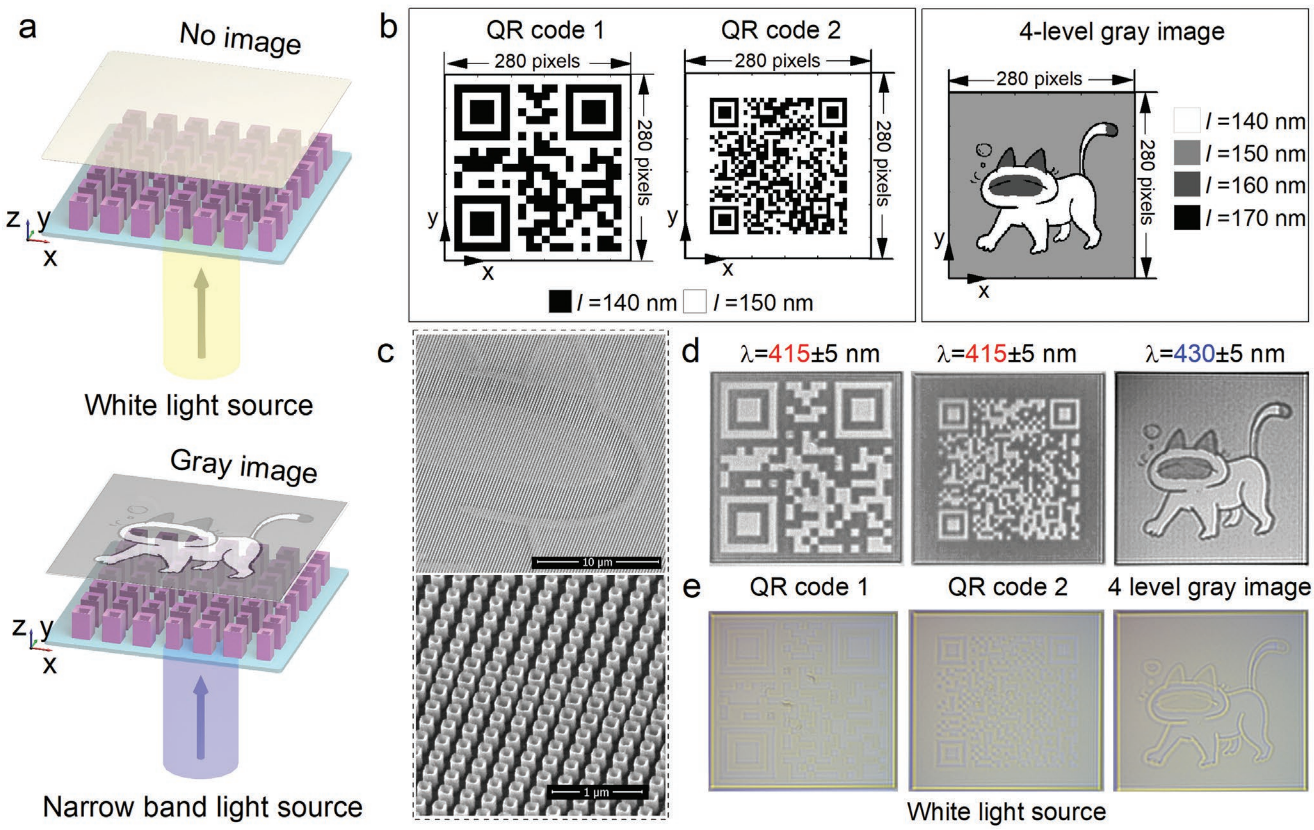

Figure 5. Realizing frequency-selective light intensity manipulation and optical encryption based on the NRH metasurfaces. a) Schematic illustrating the optical encryption strategy. No information is displayed when the designed metasurfaces is under the illumination of a white light source, while a gray image can be observed when the designed metasurface is illuminated by a narrow band light source. b) Design details of the three samples for the experimental validation of the optical encryption strategy. c) SEM images of the fabricated sample for the realization of 4-level gray image, in which the NRHs have different l and a fixed w. The captured images of the three designed samples under the illumination of d) the narrow band light source and e) the white light source.

encryption. **Figure 5**a is the schematic of the frequency-selective optical encryption based on TiO_2 metasurfaces composed of NRHs with different structural parameter l, in which the information cannot be recognized under the white illumination and can be observed with a narrow band light source. We designed three samples, as shown in Figure 5b: two of them are quick response (QR) codes with the information of the word “NKU” (QR code 1) and the website of our sample fabrication laboratory (QR code 2), and the last one is a 4-level gray image of a hand draw cat. All the three samples are composed of 280 × 280 pixels, and every pixel represents a NRH nanostructure with a given l and a fixed w. The SEM image of the fabricated sample for 4-level gray imaging is shown in Figure 5c. We can observe that the fabricated sample is composed of NRH nanostructures with different lengths l. The QR codes are designed to display the information at 410 nm and the gray image is designed to be observed at 430 nm. Owing to the slight difference between the designed and fabricated samples, the transmission spectra of the fabricated samples show a blue shift as we observed in Figure 4g. In the experiment, the wavelengths were chosen by added the narrowband interference filters with 10 nm bandwidth. With the consideration of our experimental setup, we choose the wavelengths of 415 and 430 nm for the experimental capture of the OR code images and the gray image respectively (Details in Figure S7, Supporting Information). In the experiment, the transmission intensity of the NRH metasurface with l = 140 nm is larger than that of the NRH metasurface with l = 150 nm at 415 nm, thus the captured images of the QR codes are opposite to the designed ones, as shown in Figure 5d. It does not affect the recognition of the information. The captured gray image is consistent with the designed one at 430 nm because the intensity distribution for the NRH metasurfaces with l = 140–170 nm at the wavelength of 425–430 nm in the experiment are in agreement with the simulated ones. The captured images of the QR codes and gray image in Figure 5e further prove that the intensity distribution information of the fabricated samples can be hardly recognized under the white light illumination in the transmission mode. Figure 5e also show that the colors of NRH structures with different l are slightly different. This difference is related with the difference between the measured and simulated transmission spectra in Figure 4f,g. The results in Figure 5 prove the potential use of the NRH metasurface for the realization of frequency-selective optical encryption. Part of the encoded images can be slightly observed under the white light illumination in the reflection mode, since the change of length l has a more significant effect on the reflection colors of the NRHs.

Recently, the metahologram and intensity imaging based on metasurfaces are widely used for the storage and reconstruction of image information in the far and near fields.[35,36] The former approach is mainly implemented by manipulating the phase of optical waves at the operation bandwidth, while the latter is realized by manipulating the amplitude of optical waves at the operation bandwidth. Our proposed frequency-selective optical encryption is also based on the manipulation of the amplitude of optical waves. In most previous works on metasurface enhanced grayscale imaging, the amplitude manipulation of optical waves is realized based on the Malus law, resulting in that the stored images can be observed in a broad bandwidth.[37,38] Differently, the amplitude manipulation of optical waves at the operation wavelength in our proposed approach is based on the manipulation of the resonant wavelength. Taking the advantages of the ultranarrow resonant bandwidths of the proposed NRHs, the stored images can only be observed around the resonant wavelength, which are hardly identified under white illumination. The security of the encrypted image can be further improved. Part of the encrypted image can be slightly observed under the white light illumination in the reflection mode. The structural color of the designed NRH in the reflection mode will slightly change with the variation of resonant wavelength. This can be overcome by designing the resonant wavelengths of the NRHs to be less than 380 nm. The variation of their resonant wavelength will not change structural color. Meanwhile, the encrypted channel can be expanded to multiple wavelengths and polarization states. Polarization- and wavelength-multiplexed optical encryption can be further realized by utilizing metasurfaces composed of NRHs with anisotropic optical responses and few-layer(or interleaved) NRHs, respectively. By introducing the information of decoy image in the design of polarization- and wavelength-multiplexed optical encryption based on NRH metasurfaces, the security of the encrypted image can be significantly improved.

3. Conclusion

In conclusion, we have demonstrated the use of NRH TiO_2 metasurfaces for the realization of Mie resonance confinement and manipulation in the frequency domain. We proved that the flexible confinement of Mie resonances in the frequency domain is directly related with the constraint of displacement currents in the space domain by the proposed NRH metasurfaces. With a detailed theoretical analysis, we conclude that both the refractive index and diameter of the nano hollow area play a dominate role for the confinement of the Mie resonance when the structural parameter l remains unchanged. Meanwhile, we reveal that the Mie resonance in the NRH metasurface can be fully manipulated in the whole visible regime by adjusting the structural parameters S, l, and P at the same time. On the basis of these analyses of their characteristics, we theoretically and experimentally demonstrated the potential use of the NRH metasurface in the implementation of frequency-selective intensity encoding and optical encryption. Our results provide a new and powerful approach for the manipulation and confinement of Mie resonances in the frequency domain, which can be used for the frequency-selective and -multiplexed optical manipulations.

4. Experimental Section

Sample Fabrication: TiO_2 NRH arrays with period of 250 nm were fabricated on quartz substrates by the ALAF method. The quartz substrate was cleaned in acetone, isopropanol (IPA), and deionized water in sequence. Then, the polymethyl methacrylate resist 950-A7 was spun on the quartz substrate at 3000 rpm and baked at 180 °C for 2 min. The rectangular patterns in different sizes were exposed using electron beam lithography system (6300FS, JEOL) and then were developed in a mixture of MIBK and IPA with the ratio of 1:3. Then atomic layer deposition (ALD) process was applied to deposit the TiO_2 Thin film. The ALD process of TiO_2 was carried out in a home-built ALD system. H_2O was used as the O source, and tetrakis (dimethylamino) titanium precursor was used as a Ti source to avoid chlorine contamination and heated to 75 °C to achieve the required vapor pressure. The ALD system was under continuous 20 sccm flow of N_2 carrier gas and maintained at 105 °C throughout the process. After ALD process, a dry etching process was performed in the ICP-RIE system (Plasmalab System 100 ICP180, Oxford) with a mixed reactive gas of BCl_3 and Cl_2 to remove the TiO_2 film on the top of the resist. Finally, another dry etching process with oxygen was applied to remove any residual resist.

Numerical Simulation: The numerical simulations were conducted using finite differential time domain methods. The optical constant of TiO_2 was taken from experimentally measured data (Figure S8, Supporting Information) and the refractive index of SiO_2 was taken as 1.47. The periodic boundary conditions were set in the x and y directions representing a periodical structure, and the waveguide ports boundary was defined in the z direction for light incidence and transmission while the excitation source was an x-polarized plane wave.

Experimental Measurement: The experimental measurement of the proposed NRH metasurface was based on the custom-built setup (shown in Figure 5a). A bromine tungsten lamp (Zolix, LSH-150) collimated by a fiber collimator were used as light source for the measurement of the transmission spectrum. The collected beam passed through a 4f-system formed by two lenses with an aperture set near the focus that was used to adjust the spot size of the light. Then the beam was focused on the sample with an objective (Sigma EPL 5×, NA = 0.13). The output light from the sample was collected with the other objective (Sigma EPL 50×, NA = 0.55). Then the light beam passed through a lens and a broadband unpolarized prism (MFOPT, OQNP20N-VIS), and collected by an optical spectrum analyzer (Zolix, Omni-λ3007) via a fiber coupler and a CCD camera (TUCSEN, ISH-130). For the measurement of the color images, a coaxial parallel white light source (CST Machine Vision, CST-COPS30-W, Color temperature: 5000–10 000K) was used as the light source, and the output light from the second objective was directly collected by the CCD camera. To measure the gray images at different wavelengths, narrowband interference filters (MFOPT, M-415FS10-25 and M-430FS10-25) were added in front of the CCD camera.

Supporting Information

Supporting Information is available from the Wiley Online Library or from the author.

Acknowledgements

Z.L., G.G., and J.C. contributed equally to this work. Z.L. thanks Yifan Dong for providing the hand draw cat picture. This work was supported by the National Key Research and Development Program of China (2021YFA1400601 and 2017YFA0303800), the National Natural Science Fund for Distinguished Young Scholars (11925403), the National Natural Science Foundation of China (12122406, 12192253, 11974193, 11904181, 11904183, and 91856101), the Natural Science Foundation of Tianjin for Distinguished Young Scientists (18JCJQJC45700), and the China Postdoctoral Science Foundation (2018M640224 and 2021M690084). J.L. acknowledges the financial support received from the National Natural Science Foundation of China (Grant No. 12074420).

Conflict of Interest

The authors declare no conflict of interest.

Data Availability Statement

The data that support the findings of this study are available from the corresponding author upon reasonable request.

Keywords

dielectric metasurfaces, Mie resonances, nano rectangular hollows, optical encryption, resonance confinement

Received: January 26, 2022
Revised: March 21, 2022
Published online:

[1] S. Jahani, Z. Jacob, *Nat. Nanotechnol.* **2016**, *11*, 23.
[2] W. Liu, Z. Li, H. Cheng, S. Chen, *iScience* **2020**, *23*, 101868.
[3] I. Staude, J. Schilling, *Nat. Photonics* **2017**, *11*, 274.
[4] S. Kruk, Y. Kivshar, *ACS Photonics* **2017**, *4*, 2638.
[5] K. Koshelev, Y. Kivshar, *ACS Photonics* **2020**, *8*, 102.
[6] X. Luo, *Adv. Mater.* **2019**, *31*, 1804680.
[7] S. Sun, Q. He, J. Hao, S. Xiao, L. Zhou, *Adv. Opt. Photonics* **2019**, *11*, 380.
[8] W. T. Chen, F. Capasso, *Appl. Phys. Lett.* **2021**, *118*, 100503.
[9] S. Chen, Z. Li, W. Liu, H. Cheng, J. Tian, *Adv. Mater.* **2019**, *31*, 1802458.
[10] W. T. Chen, A. Y. Zhu, F. Capasso, *Nat. Rev. Mater.* **2020**, *5*, 604.
[11] M. Liu, P. Huo, W. Zhu, C. Zhang, S. Zhang, M. Song, S. Zhang, Q. Zhou, L. Chen, H. J. Lezec, A. Agrawal, Y. Lu, T. Xu, *Nat. Commun.* **2021**, *12*, 2230.
[12] L. Wang, S. Kruk, H. Tang, T. Li, I. Kravchenko, D. N. Neshev, Y. S. Kivshar, *Optica* **2016**, *3*, 1504.
[13] B. Wang, F. Dong, Q. T. Li, D. Yang, C. Sun, J. Chen, Z. Song, L. Xu, W. Chu, Y. Xiao, Q. Gong, Y. Li, *Nano Lett.* **2016**, *16*, 5235.
[14] Y. Yang, W. Wang, A. Boulesbaa, I. I. Kravchenko, D. P. Briggs, A. Puretzky, D. Geohegan, J. Valentine, *Nano Lett.* **2015**, *15*, 7388.
[15] K. Frizyuk, E. Melik-Gaykazyan, J. H. Choi, M. I. Petrov, H. G. Park, Y. Kivshar, *Nano Lett.* **2021**, *21*, 4381.
[16] G. Li, S. Zhang, T. Zentgraf, *Nat. Rev. Mater.* **2017**, *2*, 17010.
[17] X. Liu, Z. Huang, J. Zang, *Nano Lett.* **2020**, *20*, 8739.
[18] W. Yang, S. Xiao, Q. Song, Y. Liu, Y. Wu, S. Wang, J. Yu, J. Han, D. P. Tsai, *Nat. Commun.* **2020**, *11*, 1864.
[19] F. Yesilkoy, E. R. Arvelo, Y. Jahani, M. Liu, A. Tittl, V. Cevher, Y. Kivshar, H. Altug, *Nat. Photonics* **2019**, *13*, 390.
[20] N. A. Rubin, G. D'Aversa, P. Chevalier, Z. Shi, W. T. Chen, F. Capasso, *Science* **2019**, *365*, 43.
[21] M. L. Tseng, Y. Jahani, A. Leitis, H. Altug, *ACS Photonics* **2020**, *8*, 47.
[22] S. D. Rezaei, Z. Dong, J. Y. E. Chan, J. Trisno, R. J. H. Ng, Q. Ruan, C.-W. Qiu, N. A. Mortensen, J. K. Yang, *ACS Photonics* **2020**, *8*, 18.
[23] A. Tittl, A. Leitis, M. Liu, F. Yesilkoy, D. Y. Choi, D. N. Neshev, Y. Kivshar, H. Altug, *Science* **2018**, *360*, 1105.
[24] G. Yoon, D. Lee, K. T. Nam, J. Rho, *ACS Nano* **2018**, *12*, 6421.
[25] S. I. Azzam, A. V. Kildishev, *Adv. Opt. Mater.* **2021**, *9*, 2001469.
[26] C. W. Hsu, B. Zhen, A. D. Stone, J. D. Joannopoulos, M. Soljačić, *Nat. Rev. Mater.* **2016**, *1*, 16048.
[27] D. Ma, Z. Li, Y. Zhang, W. Liu, H. Cheng, S. Chen, J. Tian, *Opt. Lett.* **2019**, *44*, 3805.
[28] K. V. Baryshnikova, D. A. Smirnova, B. S. Luk'yanchuk, Y. S. Kivshar, *Adv. Opt. Mater.* **2019**, *7*, 1801350.
[29] B. Yang, W. Liu, Z. Li, H. Cheng, D. Y. Choi, S. Chen, J. Tian, *Nano Lett.* **2019**, *19*, 4221.
[30] G. Geng, W. Zhu, R. Pan, Z. Zhang, C. Gu, J. Li, *Nano Today* **2021**, *38*, 101145.

[31] P. C. Wu, C. Y. Liao, V. Savinov, T. L. Chung, W. T. Chen, Y. W. Huang, P. R. Wu, Y.-H. Chen, A.-Q. Liu, N. I. Zheludev, D. P. Tsai, *ACS Nano* **2018**, *12*, 1920.
[32] V. Savinov, V. A. Fedotov, N. I. Zheludev, *Phys. Rev. B* **2014**, *89*, 205112.
[33] J. Xue, Z. K. Zhou, L. Lin, C. Guo, S. Sun, D. Lei, C.-W. Qiu, X. H. Wang, *Light: Sci. Appl.* **2019**, *8*, 101.
[34] D. Franklin, S. Modak, A. Vázquez-Guardado, A. Safaei, D. Chanda, *Light: Sci. Appl.* **2019**, *7*, 93.
[35] I. Kim, G. Yoon, J. Jang, P. Genevet, K. T. Nam, J. Rho, *ACS Photonics* **2018**, *5*, 3876.
[36] L. Deng, J. Deng, Z. Guan, J. Tao, Y. Chen, Y. Yang, D. Zhang, J. Tang, Z. Li, Z. Li, S. Yu, G. Zheng, H. Xu, C.-W. Qiu, S. Zhang, *Light: Sci. Appl.* **2020**, *9*, 101.
[37] F. Yue, C. Zhang, X. F. Zang, D. Wen, B. D. Gerardot, S. Zhang, X. Chen, *Light: Sci. Appl.* **2018**, *7*, 17129.
[38] Z. Li, W. Liu, H. Cheng, D. Y. Choi, S. Chen, J. Tian, *Adv. Opt. Mater.* **2019**, *7*, 1900260.